

Reliability studies of micro-optical components in NEMO

F. Berghmans^{*a,b}, M. Van Uffelen^a, S. Eve^{**c}, E. Ernst^c, A. Last^d, D. Rabus^d, N. Huber^c, O. Kraft^c,
A. Andrei^e, L. Nieradko^e, K. Krupa^e, M. Jozwik^e, C. Gorecki^e, L. Hirsinger^f, P. Delobelle^f,
P. Kniazewski^g, L. Salbut^g, M. Kujawska^g

^aSCK•CEN, Boeretang 200, B-2400 Mol, Belgium;

^bVrije Universiteit Brussel, Pleinlaan 2, B-1050 Brussel, Belgium;

^cIMF II, Forschungszentrum Karlsruhe GmbH, Postfach 3640, D-76021 Karlsruhe, Germany;

^dIMT, Forschungszentrum Karlsruhe GmbH, Postfach 3640, D-76021 Karlsruhe, Germany;

^eLOPMD, FEMTO-ST, 16 Route de Gray, F-25030 Besançon, France;

^fLMARC, FEMTO-ST, 24 Chemin de l'Épitaphe F-25000 Besançon, France;

^gInstitute of Micromechanics and Photonics, Warsaw University of Technology, 8 Sw. A. Boboli,
02-525 Warsaw, Poland

ABSTRACT

We discuss on-going reliability studies of micro-optical components and assemblies as conducted in the EU FP6 Network of Excellence on Micro-Optics "NEMO". We focus on three case studies including first biaxial fatigue testing of micro-optical components, second reliability testing and quality control of MEMS and third micro-interferometric tomography for measuring optical fibre refractive index changes. For each of these case studies we discuss the dedicated measurement and characterization methods as well as first results and the perspectives for future research.

Keywords: micro-optic, reliability, fatigue, metal film, polymer, MEMS, interferometer, refractive index, optical fibre, radiation

1. INTRODUCTION

The reliability of a product (device, module or system) can be defined as the probability that this product will perform a certain function within a set of pre-defined specifications for a given period in time. A manufacturer needs to guarantee the correct operation of his products for a certain time. It is therefore essential to know the reliability of these products since this has a fundamental influence on the competitiveness and on the acceptance of a technology. Extensive reliability studies have been conducted for many materials (metals, glasses, plastics, dielectrics, ceramics, adhesives, etc.) and for a large range of products (micro-electronics, opto-electronics, electrical devices, mechanical components, optical fibres, etc.). However, these studies did not necessarily focus on the issues that appear when the materials and products are processed and integrated in micro-optical functional devices. In addition, new types of materials are being engineered and integrated in novel ways to yield paradigm shifting micro-optical devices, for which new or adapted reliability assessment methods need to be developed.

Such devices, their manufacturing technologies and their applications form the centre of gravity of the activities conducted within the EU FP6 Network of Excellence on Micro-Optics – "NEMO"¹. Micro-optics is a generic technology that allows the manipulation of light and the management of photons with "micron"- and "sub-micron"-scale structures and components. Micro-optics is therefore the corner-stone enabling technology to interface the macroscopic world we live in with the microscopic world of opto- and nano-electronic data processing circuits. It is recognized as the key-link between photonics and nano-electronics, the two dominating information technologies in tomorrow's society.

NEMO aims at providing Europe with a complete Micro-Optics food-chain by setting up durable service and technology centres for Optical Modelling and Design; Measurement and Instrumentation, Mastering, Prototyping and Replication; Hybrid Integration and Packaging; Reliability and Standardization. NEMO's main objective is to structure and integrate the expertise and core-competences of its partners while strengthening their R&D activities in the emerging fields of micro-optics.

* francis.berghmans@sckcen.be; phone 32 14 332637; fax 32 14 311993; www.sckcen.be

** S. Eve is now with ESCTM du CRISMAT – ENSICAen, 6 Boulevard Maréchal Juin, F-14050 Caen Cedex, France

This brings us to the objective of this paper which is to summarize part of the work conducted on the reliability assessment of selected micro-optical materials, devices and related methods within NEMO. The paper is articulated around three case studies carried out as a collaboration between several NEMO partners, i.e. biaxial fatigue testing of micro-optical components; reliability testing and quality control of MEMS and, finally, micro-interferometric tomography for measuring optical fibre refractive index changes. For each of these case studies we discuss the dedicated measurement and characterization methods as well as preliminary results and the perspectives for future research.

2. CASE STUDY 1 : BIAXIAL FATIGUE TESTING OF MICRO-OPTICAL COMPONENTS

2.1. Introduction

A current trend in micro-optics is to develop micro-devices based on polymer substrates, which offer manufacturing flexibility and possible cost effective production. Some innovative micro-optical components relying on submicron films of metal deposited on micro-structured polymer substrate are currently implementing mirroring and waveguiding functionalities²⁻⁴. During their application these components experience thermal cycling. Since film and substrate have different thermal expansion coefficients size mismatches appear which must be accommodated, for the largest part, by the film. This results in high residual stresses and in deformation leading to roughening, delamination and cracking of the film (Fig. 1). To assess the reliability of such devices one could rely on the ISO 9022-2 norm, which recommends a thermal test consisting of 5 cycles between -40°C to $+55^{\circ}\text{C}$. This test takes several hours and only characterizes the low cycle fatigue behaviour of the components under extreme conditions. It can therefore not be used to predict the lifetime of micro-optical components. Instead, replacing the thermal cycling by a mechanical cyclic loading which reproduces the biaxial loading conditions created by temperature variations allows separating the thermally and mechanically affected deformation mechanisms. In addition it yields a significant acceleration of the test. This method has been applied to investigate the fatigue behaviour of gold film deposited on PMMA (PolyMethylMethAcrylate) and PC (PolyCarbonate) substrates.

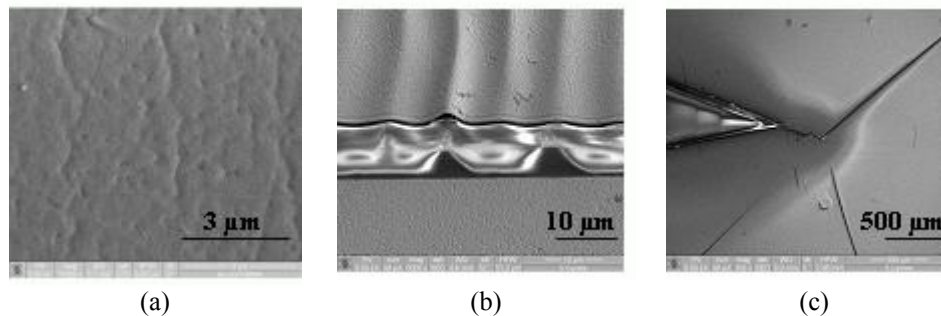


Figure 1: SEM micrographs of different types of damage observed in a micro-spectrometer element (400 nm thick gold film on 1.28 mm thick PMMA substrate) after a thermal cycling according to the ISO 9022-2 norm: (a) roughening, (b) delamination and (c) cracking of the film.

2.2. Experimental methods

We have developed a new experimental set-up, which allows applying a biaxial loading in agreement with the situation during thermal loading. It is based on the ring-on-ring test, which has been successfully applied to other materials, particularly for strength measurements on glass and ceramics⁵⁻⁷. In this test, the specimen is supported by a ring while a smaller concentric ring loads the opposite face. It produces a biaxial tensile strain and stress state inside the smaller ring, which is identical to that applied by thermal heating. We have modified the conventional set-up in order to allow the mechanical simulation of thermal fatigue test with alternating tensile and compressive strain in the film. Support and loading rings are applied on both sides of the specimen (Fig. 2a). In our configuration, the specimen is clamped by the inner rings, which are fixed, and loaded by the outer rings, connected to the crossbeam of the testing machine. Having the specimen with the film at the top side, a tensile stress is applied on the film when the loading rings are pushed downwards, while a compression stress is applied when they are pulled upwards.

The fatigue experiment is completed by an in-situ failure detection method. It is based on the fact that the main property of the metal film in its application is its optical reflectivity, which decreases when the film is damaged. As soon as

damage occurs, some light would be dispersed by the surface. This can be detected by a set of photodiodes located in front of the film, outside of the main reflection. This system, which is placed in front of the film inside the inner ring (Fig. 2a), comprises four small photodiodes, which are surrounding a hole for the laser beam (Fig. 2b). Due to the restriction of space inside the inner ring, the light beam hits the film surface with an angle of 90° , so that the incoming and reflected beams are superposed.

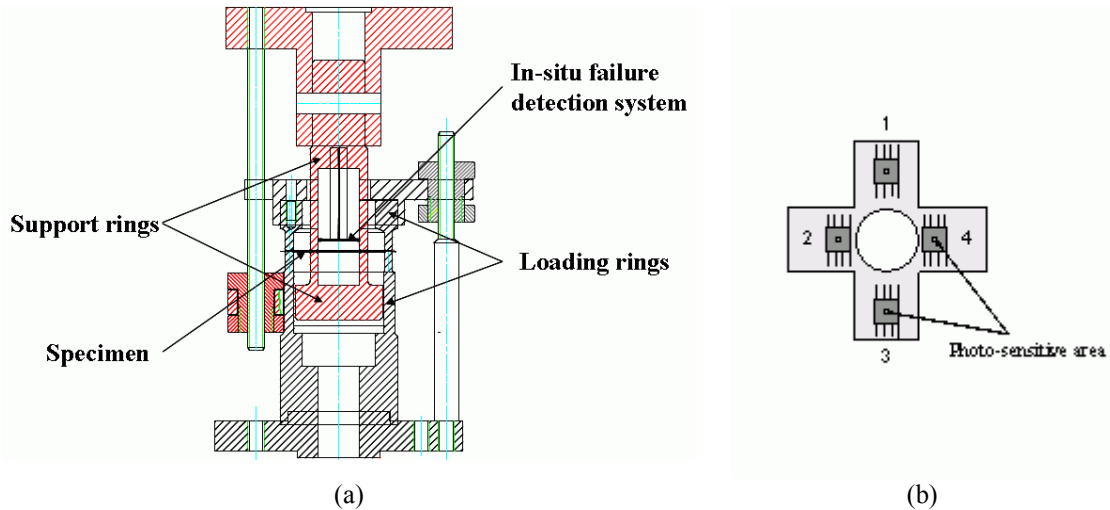


Figure 2: (a) Cross section of the mechanical set-up. (b) The in-situ damage detection system.

In this study, we have performed thermal tests on micro-optical components of gold deposited on PMMA or PC substrates, with film and substrate thickness of 400 nm and 1.28 mm respectively. These micro-optical components with 3D microstructures are produced by hot-embossing of the polymer and physical vapour deposition of the reflective films. According to the same processes, and considering the same material combinations, flat samples for the mechanical tests have been produced by IMT/FZK. These specimens, designed for our experimental set-up, are circular with a diameter of 70 mm, and have the same film and substrate thicknesses (400 nm and 1.28 mm respectively) as the micro-optical components.

Micro-optical elements have been thermally cycled in a climate chamber, according to the ISO 9022-2 norm (5 cycles between -40°C to $+55^\circ\text{C}$, with a rate of $0.7^\circ\text{C}/\text{min}$, and hold periods of 2.5 h at the minimum and maximum temperatures). The mechanical tests were conducted on two servo hydraulic testing machines, equipped with load cells of 10 and 40 kN, under load control, at room temperature and one frequency (0.2 Hz). The strain in the specimen during the test is measured using a deformation gauge, glued on the specimen in the opposite side to the coating. The strain amplitude corresponding to the standard temperature change test between -40°C and $+55^\circ\text{C}$ has been determined by 2D finite element calculations, using the commercially available software ABAQUS. Table 1 summarizes the strain in the film related to a decrease of the temperature from $+20^\circ\text{C}$ to -40°C , and for an increase from 20°C to $+55^\circ\text{C}$. To study the influence of the strain amplitude applied to the specimen, we have performed mechanical tests with strain amplitudes of 25%, 50% and 100% of the strain amplitude corresponding to a standard thermal cycle (Tab. 1).

	Au on PC	Au on PMMA
$\Delta\alpha_{20^\circ\text{C}} (\text{C}^{-1})$	$5.1 \cdot 10^{-5}$	$5.4 \cdot 10^{-5}$
$\Delta\epsilon_{+20 \rightarrow -40^\circ\text{C}} (\%)$	-0.376	-0.397
$\Delta\epsilon_{+20 \rightarrow +55^\circ\text{C}} (\%)$	+0.220	+0.232

Table 1: Expansion coefficient difference and strain amplitude in the metal film due to a temperature changes between -40°C to $+55^\circ\text{C}$, to which we refer as standard thermal test.

The fatigue damage is characterized using scanning electron microscopy (SEM), and a FEI 200xP dual beam focused ion beam (FIB) work station. After a fixed number of mechanical cycles, depending on the strain amplitude (each 500

cycles for a strain amplitude of 100%, each 5000 cycles for the other strain amplitudes), the specimen was removed from the set-up and the film surface was examined.

2.3. Results

Figure 3 shows the evolution of film damage of an Au/PC specimen, loaded with a strain amplitude corresponding to a standard thermal cycle. Until 1000 cycles, only some localized surface damage is visible, which is considered as manufacturing defects. After 1000 cycles, roughening starts to develop on the film, and after 1500 cycles, cracks and extrusions are occurring. FIB cross-sectional views show the delamination of the metal film, and the formation of voids at the film/substrate interface underneath the extrusions. This film damage is similar to that observed after a thermal cycling. The number of cycles, at which damage occurs, depends on the applied strain amplitude (Fig. 4b).

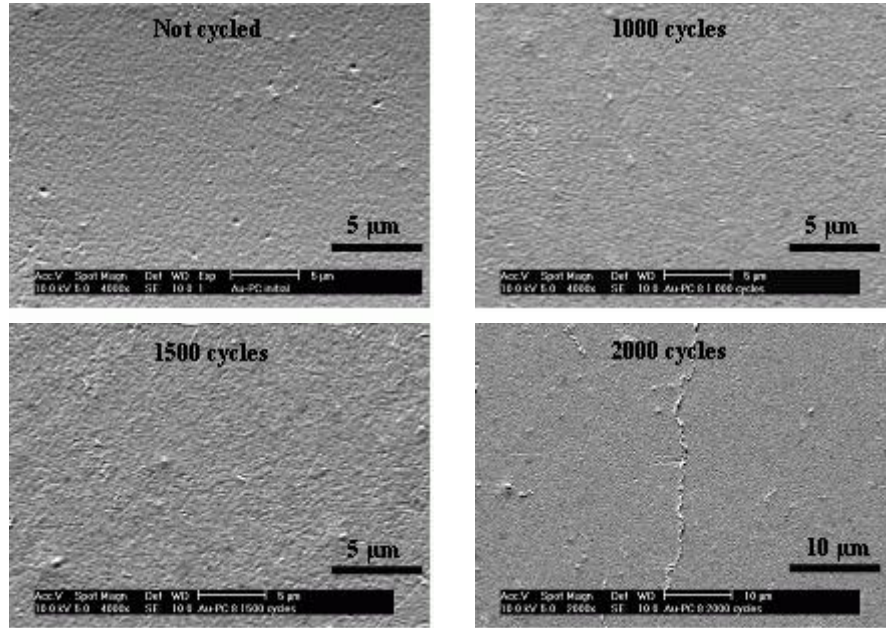


Figure 3: SEM micrographs of the evolution of the surface damage of an Au/PC specimen, loaded with a strain amplitude corresponding to a standard thermal cycle.

Figure 4a presents the output voltage of the in-situ detection system as a function of the number of cycles for the Au/PC specimen. No significant change in the output voltage of the sensor is detected until 1400 cycles. After this point, we note a slight decrease of the output voltage. After 1550 cycles, a series of peaks is recorded. Comparing these data to the SEM observations the continuous decrease of the output voltage of the detection system has been correlated to the beginning of the roughening of the film, and the peaks to the appearance of cracks and extrusions. Figure 4b compares the number of cycles to damage determined from SEM observations (open triangles: no damage observed, full triangles: damage observed) and from the output data of the in-situ system (circles: open symbols correspond to the beginning of the decrease in the output voltage, filled symbol to the apparition of peaks). The reasonable agreement shows that our detection system possesses sufficient sensitivity and allows distinguishing the different types of damage.

Moreover, we have observed that the output voltage of the detection system shows a slight increase at the beginning of the mechanical fatigue for all the specimens (Fig. 5a). A decrease of the output voltage is correlated to an increase of the film roughness, so that such an increase of the output voltage would correspond to a decrease of the film roughness. This increase in the first stage was unexpected and AFM measurements were performed on specimens at different defined locations, before and after cyclic loading. The tests were interrupted as soon as the output voltage of the detection system increased. As an example, figures 5a and 5b show the evolution of the sensor output voltage and the average roughness R_a , respectively, of an Au/PMMA specimen loaded with a strain amplitude of 25% of the standard thermal cycle. The clear decrease in roughness, as determined by AFM, correlates with the sensor output voltage, which confirms the sensitivity of our method.

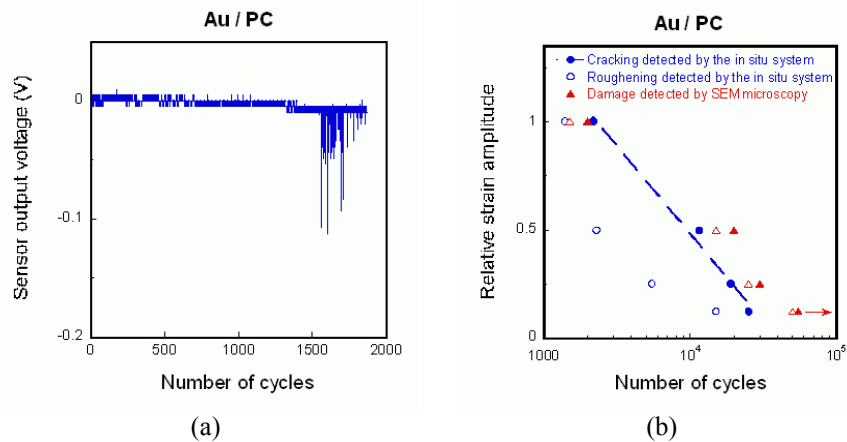


Figure 4: (a) Evolution of the output voltage of the photo sensors during a mechanical test of the Au/PC specimen as a function of the number of cycles. (b) Influence of the relative strain amplitude on the number of cycles to damage. Comparison between the onsets of damage determined by SEM observations and by the in-situ system.

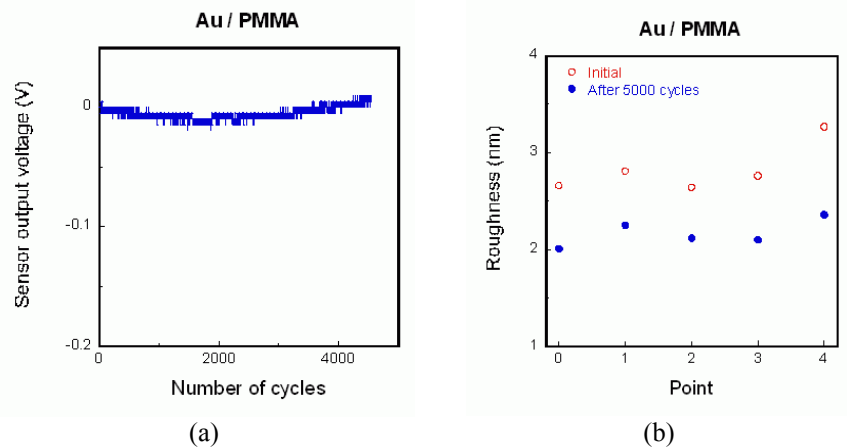


Figure 5: (a) Evolution of the output voltage of the photo sensors during the first 5000 cycles of a mechanical test on an Au/PMMA specimen, loaded with a relative strain amplitude of 25%, as a function of the number of cycles; (b) AFM measurements of the film roughness R_a before and after 5000 cycles.

2.4. Conclusion

We have investigated the thermal and mechanical fatigue behaviour of submicron gold films on polymer substrates (PC and PMMA), in terms of material combinations and type of damage produced. We have developed a new experimental set-up, which allows reproducing the biaxial loading created by thermal cycling. This set-up is completed by an in-situ failure detection system, which is able to identify with a good sensitivity the two damage mechanisms, which are roughening and further occurrence of cracks and extrusions. The influence of the temperature on the fatigue behaviour of our specimens will be investigated by adding a heating system on the mechanical set-up.

3. CASE STUDY 2 : RELIABILITY TESTING AND QUALITY CONTROL OF MEMS

3.1. Introduction

Aluminium nitride (AlN) is a promising material for many MEMS/MOEMS applications. The piezoelectric properties of AlN films are mostly exploited for bulk acoustic wave propagation in miniature high frequency bypass filters for the

ever-growing wireless communication market^{8,9}. In the field of Micro-Electro-Mechanical Systems (MEMS), sensors using surface acoustic waves have already been proposed^{10,11}. However, the use of AlN films as an actuation layer is more uncommon¹². That brings us to the objectives of this case study, i.e. to develop reliable AlN driven micro-cantilevers working as actuation elements in MEMS and to contribute to the understanding and analysis of MEMS failure processes. Understanding the failure physics of MEMS is quite complex as multiple materials and interfaces are involved that all influence the ways in which the system interacts with the local environment. This characteristic brings forward the need for a thorough study of the role of cyclic fatigue and environmental factors in the reliability assessment of MEMS. In what follows we therefore first deal with the fabrication process of the micro-cantilevers. Second we focus on accelerated ageing through thermal cycling and on its influence on the bending of the cantilevers.

3.2. Design and fabrication of test structures

AlN driven micro-cantilevers were fabricated on 3", 380 μm thick, (100) oriented Si wafers. Figure 6 shows the flow-chart of the process. After realising a 15 μm thick Si membrane by KOH etching of one side of the wafer (step 1), three thin layers are successively deposited on the other side in order to form a metal 1 / AlN / metal 2 stack (steps 2,3 and 4). Metal 1 is a CVD 150 nm thick Aluminium layer. The AlN is deposited in a reactive pulsed DC sputtering machine. The input power was 150 Watt leading to a relative low deposition rate of about 3 nm/min. The AlN film has a thickness of 400 nm. The second metal is a CVD 100 nm thick CrNi alloy. This alloy has been chosen for its very good resistance to reactive ion etching (RIE) of AlN performed at step 5 of the process. Therefore, the shape of the final micro-beams is defined by this metal 2 layer used as a hard mask : 50 μm width and a length between 100 and 1000 μm. The AlN etch stops on the bottom metal electrode. A third thick (500 nm) Aluminium layer (metal 3 at step 6) has been deposited and patterned in order to form wire-bonding pads. At this moment, the CrNi / AlN / Al sandwich is already defining the beam pattern over the Si membranes. The last dry RIE step will finally remove the silicon which is not under the beam pattern, transforming the initial Si membranes into a network of free standing cantilevers as they are presented in the layout (Fig. 6).

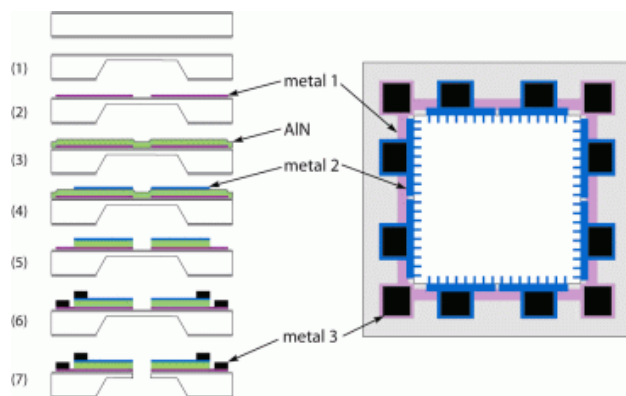


Figure 6 : Flow chart and layout of the AlN driven cantilevers.

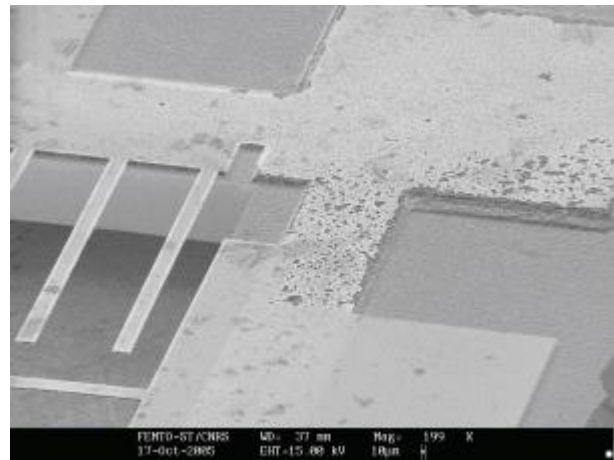


Figure 7 : Example of bottom electrode damage due to the low resistance of the metal 1 layer to the AlN RIE process step.

3.3. Results

The choice of the metals for the top and bottom electrodes proved to be a delicate matter, as the metal layers must have a very good resistance to the AlN etch step. The use of an CrNi alloy as the top electrode and hard mask for AlN RIE gave good results. Unfortunately, this is not the case for the metal 1 layer (aluminium) that showed a much lower resistance to RIE (Fig. 7).

Furthermore, as one could expect for a CVD process, the thicknesses of the thin films were not uniform over the wafer. The AlN thickness was 20% larger in the centre of the wafer compared to the edge. The same holds for the metal layers that showed differences in thickness of about 15% between the centre and the edge.

Residual stresses have also been evaluated using test cantilevers specially designed for process control. The aluminium film shows a relatively low compressive stress of about -50 MPa. The CrNi showed a high tensile residual stress of about 700 MPa. The AlN film was also found to have a tensile residual stress of about 300 MPa. Given the low power deposition conditions this result is in good agreement with literature¹³.

In order to evaluate the long term stability, the influence of temperature on the behaviour of the cantilevers has been studied. The measurement system is based on a Twyman-Green interferometer¹⁴ and uses phase-shift algorithms¹⁵. This allows finding both static (initial shape, out-of-plan displacements) and dynamic parameters of the cantilevers (e.g. resonance frequencies and amplitude distributions in vibration modes). We need to emphasize that the micro-beam fabrication process has an influence on the flatness and on the initial shape of the micro-structures. The deposition and etch of multiple thin layers on an initially straight Si introduce internal stresses and generate bending. Therefore, the initial static shape of the AlN micro-beams was determined before starting the thermal test. After this initial characterization, the samples were kept at 130°C in vacuum for 87 hours. The vacuum was necessary to avoid possible deteriorations of the devices stemming from metal oxidation due to the environmental humidity. The measurement results are summarised in Table 2. The values of the initial deflection were averaged over 10 cantilevers of each studied length. The results from the initial deflection measurements of the exemplary 700 µm cantilever are shown in figure 8a and the changes after the thermal treatment in figure 8b. Preliminary results show that the initial displacements decrease upon thermal ageing. This stems from an internal stress relaxation with an estimated stress change value of 2%.

Cantilever length [µm]	Initial deflection [nm]		Changes of initial deflection [nm]	Percentage changes of initial deflection [%]
	before T=130 °C	after T=130 °C		
200	1129,1	941,5	187,5	16,6
500	3659,2	3491,8	167,4	4,6
700	13483,8	13010,6	473,3	3,5

Table 2: Results of static deflection measurements.

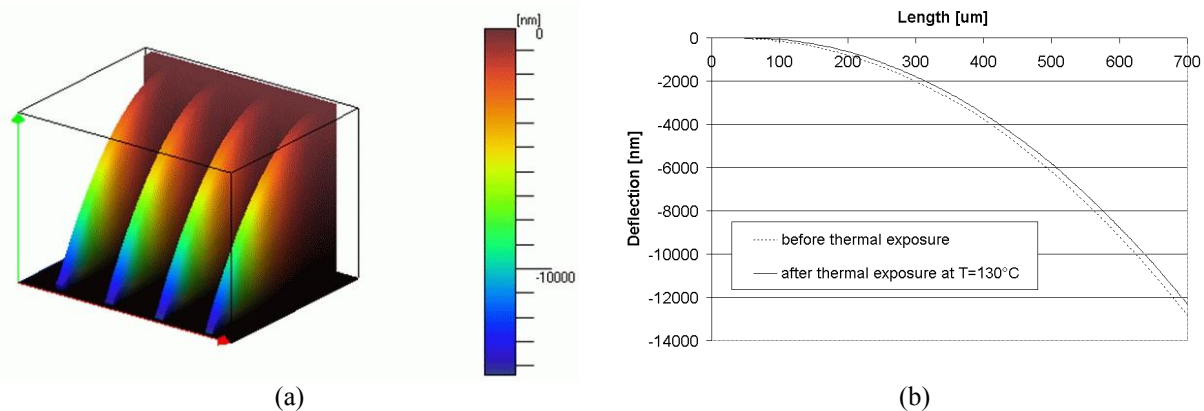


Figure 8: The initial deflection for 700 µm long cantilever : (a) 3D representation; (b) comparison of cross-sections before and after thermal treatment at 130 °C.

3.4. Conclusion

The ability to experimentally characterize static and dynamic deformation effects is crucial to the development of actuated MEMS devices and micro-optical systems. Accurate metrology indeed plays a key role in the characterization and control of critical micro-machining processes. We illustrated this with actuators for micro-mechanical applications using an AlN piezoelectric layer. For characterizing these structures we relied on an interferometric platform. Preliminary experiments indicate that temperature has an influence on the initial deflection of the cantilevers. Temperature treatment seems to release internal stresses which decrease static deflections. The largest changes of deflection were observed for shorter cantilevers. Future work will focus on improving the technological fabrication process, on reliability studies of the dynamical parameters and on life time predictions of the AlN micro-cantilevers.

4. CASE STUDY 3 : MICRO-INTERFEROMETRIC TOMOGRAPHY FOR MEASURING OPTICAL FIBRE REFRACTIVE INDEX CHANGES

4.1. Introduction

Optical fibre technology finds applications in different environments where the presence of ionizing or particle radiation is of concern, for example in space, in nuclear industry and in high energy physics experiments, either for communication or for sensing purposes. It is well known that highly energetic radiation increases the absorption in glass optical fibres by introducing so-called colour centres. Radiation induced colour centres and defects in glass materials have been investigated for almost 50 years. Other optical phenomena which have been studied, albeit to much lesser extent, include radiation induced luminescence and radiation induced refractive index changes in glass^{16,17}.

The latter are nevertheless important as they may alter the wave guiding properties of optical fibres and therefore influence the design and the reliability of fibre based instruments such as optical fibre sensors for nuclear industry or for space applications, fibre-optic spacecraft gyroscopes, high speed intra-satellite links, space LIDARs and others. On the other hand, understanding highly energetic radiation induced refractive index changes might open prospects for the fabrication of glass based photonic integrated circuits using, for example, focused ion beams. Although a considerable amount of knowledge has been developed for UV-radiation induced refractive index changes, which is the basis for the fabrication of fibre Bragg gratings, no systematic study was conducted for the case of highly energetic radiation such as gamma-rays and accelerated protons or other ions. A number of results reported in open literature evidence that the typical radiation induced refractive index changes are overall relatively low. These results should nevertheless be intercompared with specific care as they come with different sample materials, radiation conditions, measurement wavelengths, measurement geometries and accuracies.

4.2. Experimental method

Micro-interferometric tomography is a full-field method that allows determining a three-dimensional refractive index distribution $n(x,y,z)$ ¹⁸. It combines laser interferometry with tomographic 3D reconstruction methods¹⁹ and proved to be an excellent tool for analyzing $n(x,y,z)$ in a large variety of phase micro-elements including optical fibre based samples²⁰, gradient index lenses and waveguides with modified refractive index distributions. The set-up of the automated micro-interferometric tomograph used for our experiments and which relies on a Mach-Zehnder interferometer is depicted in figure 9. A He-Ne laser beam is coupled into a polarization maintaining single mode optical fibre with microscopic objective OB1. To adjust the polarization to the proper axis of the fibre a half wave plate $\lambda/2$ is placed between the source and the objective OB1. A coupler S divides the light into object and reference beams, the linear polarization of light being maintained by the coupler and the fibre. To avoid refraction of the object beam the measured sample is placed in a dedicated cuvette filled with a refractive index matching liquid. A computer controlled rotation stage rotates the sample with an accuracy of $1/200^\circ$. The radial run-out of the rotation stage is $\pm 1 \mu\text{m}$. The imaging system consists of a microscopic objective OB5 (20x, infinite-type correction), a cube-splitter BS and a lens L ($f=400$) conjugated with a 1376x1035 CCD camera. The camera covers a field of view of $191 \times 144 \mu\text{m}^2$. The spatial resolution of the projections taken by the optical system is $0.12 \mu\text{m}$. The complete optical set-up is controlled with a computer managing both the measurement with data acquisition and data analysis, the latter including interferogram analysis and tomographic reconstruction. A measurement cycle consists of the following stages:

1. acquisition of the interferograms for each sample position (in the case presented below 180 frames were taken, i.e. with successive rotation steps $\Delta\alpha = 1^\circ$);
2. phase calculation for each interferogram²¹;
3. reconstruction of the 3D phase distribution (modified filtered back projection method) and its scaling to the refractive index distribution;
4. adjusting the position of the distribution referring to the known value of the immersion liquid refractive index to obtain the absolute value of the refractive index.

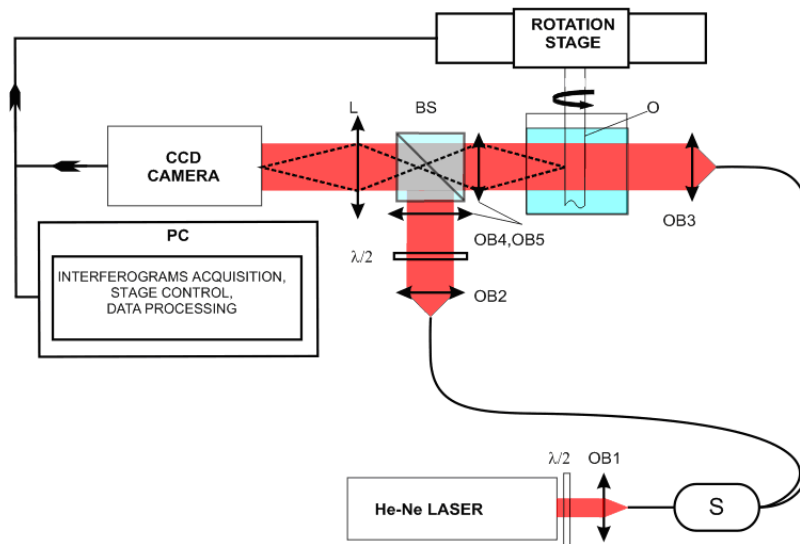


Figure 9: Automated tomographic micro-interferometer : $\lambda/2$ – halfwave plate; OB1, OB2, OB3 – fibre coupling objectives; OB4, OB5 – imaging objectives; L – camera objective; O – sample; K – cuvette with index matching liquid; BS – cube splitter; S – fibre coupler.

4.3. Results

The samples for our experiments were short lengths (about 10 cm) of standard Corning SMF-28 fibre. A number of samples taken from the same fibre spool were irradiated up to total doses of respectively 0.5 MGy and 5.0 MGy, at a dose-rate of 23 kGy/h, using the BRIGITTE ^{60}Co immersed gamma irradiation facility at SCK•CEN (Belgium)²².

The measurements of the refractive index distribution were performed for seven samples for each cumulated dose (0.5 MGy and 5.0 MGy) and compared to the refractive index measured on pristine fibre. In order to provide absolute values of the refractive index, the known value of the refractive index of a certified immersion liquid is taken as the reference. This value is then assigned to the refractive index in the immersion liquid area in the relative phase distribution. This yields the absolute refractive index distribution at the measurement wavelength $0.6328 \mu\text{m}$.

Figure 10 shows the reconstructed refractive index profile over a cross section of the fibre. The averaged refractive index values in the core and cladding are summarized in Table 3.

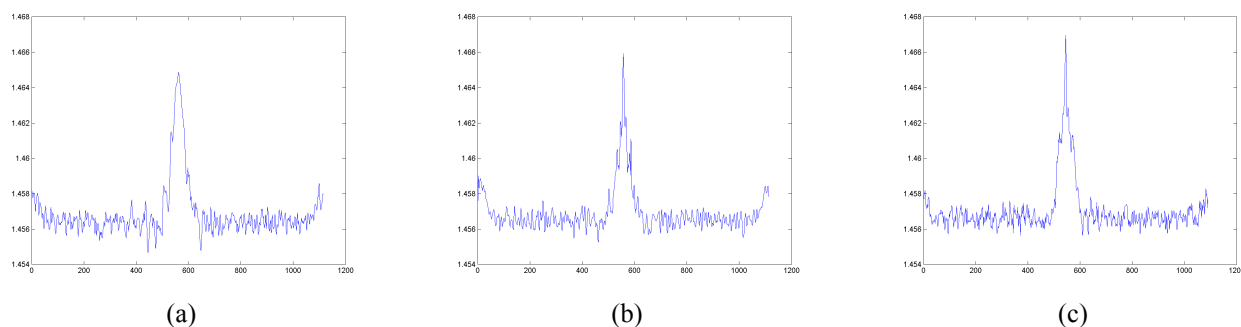


Figure 10: Measured refractive index profiles for different total doses. The horizontal axis gives the pixel number and the vertical axis gives the absolute refractive index. (a) Pristine fibre; (b) 0.5 MGy total dose; (c) 5.0 MGy total dose.

The refractive index changes due to the irradiation appear to be different for the core and cladding. This can be explained by the difference in the core and cladding material. In the core area the change of the refractive index after a dose of 0.5 MGy equals 0.0010, while after 5 MGy this change increases to 0.0013. In the cladding this change is one

order of magnitude smaller, but seems still present. The changes measured by tomographic interferometry are of the same order of magnitude of those reported in literature.

	Pristine fibre	0.5 MGy total dose	5.0 MGy total dose
Core	1.4640	1.4650	1.4653
Cladding	1.4563	1.4563	1.4565

Table 3: Averaged refractive indices in core and cladding.

4.4. Conclusion

We presented a method that allows to measure variations in the local distribution of the refractive index in single mode optical fibres. Micro-interferometric tomography seems sensitive enough to distinguish the differences between irradiated and pristine optical fibres or other types of glass samples. For the application considered here this method has the following advantages :

- it returns the material refractive index at the measurement wavelength, and not the modal or any averaged refractive index ;
- it returns the difference between the core and cladding refractive index and therefore the change in guidance properties ;
- the measurements can be conducted on many samples. Therefore results with statistical significance can be obtained.

A major disadvantage remains that the measurements can not be conducted in-situ, i.e. during the irradiation, and only at irregular time intervals after the irradiation. Therefore post-irradiation recovery and the kinetics of the processes are not taken into account. Future work will include an optimization of the micro-interferometric tomography to improve the refractive index measurement accuracy and a more systematic study of the effect of radiation on the refractive index of various types of glass fibres and materials.

5. SUMMARY

We reported on reliability studies conducted within the EU FP6 Network of Excellence on Micro-Optics – NEMO. These studies focus on very particular issues that apply to micro-optical devices. First we dealt with a case study that investigated the thermal and mechanical fatigue behaviour of submicron gold films on polymer substrates (PC and PMMA). Metal film on polymer substrate systems are nowadays being used as a basis for fabricating a variety of micro-optical devices, e.g. micro-spectrometers. To study the thermal and mechanical fatigue behaviour in terms of material combinations and type of damage we used a new experimental set-up which allows reproducing biaxial loading created by thermal cycling. In a second case study we looked at the behaviour of micro-cantilevers that use an AlN piezolayer to serve the actuation mechanism. Micro-cantilevers are basic elements in a variety of MEMS/MOEMS but AlN is yet not very well known as an actuating material. Here a dedicated interferometric set-up was necessary to characterise the static and dynamic deformations of these elements. Finally a third case study attempted to evidence refractive index changes in the core and cladding of single-mode optical fibres exposed to ionising radiation. Although these case studies relate to different kinds of elements, two common issues were evidenced : first the microscopic scale on which the measurements need to be conducted and with that the fundamental importance of adapted measurement and characterisation methods for assessing the reliability of novel micro-optical devices and material systems.

REFERENCES

1. <http://www.micro-optics.org>
2. N. Bowden, S. Brittain, A.G. Evans, J.W. Hutchinson and G.M. Whitesides, "Spontaneous formation of ordered structures in thin films of metals supported on an elastomeric polymer", *Nature*, **393**, pp. 146-149, 1998.
3. H. Kupfer and G.K.Wolf, "Plasma and ion beam assisted metallization of polymers and their application", *Nucl. Instrum. Meth. B*, **166-167**, pp. 722-731, 2000.
4. A. Last, H. Hein and J. Mohr, "Shape deviations in masks for optical structures produced by electron beam lithography", *Microsystem Technologies*, **10**, pp. 527-530, 2004.

5. T. Thiemeier, A. Brückner-Foit and H. Kölker, "Influence of the fracture criterion on the failure of ceramics loaded in biaxial flexure", *J. Am. Ceram. Soc.*, **74**, pp. 48-52, 1991.
6. B.J. Hulm, J.D. Parker and W.J. Evans, "Biaxial strength of advanced materials", *J. Mater. Sci.*, **33**, pp. 3255-3266, 1998.
7. M.H. Krohn, J.R. Hellmann, D.L. Shelleman and C.G. Pantano, "Biaxial flexure strength and dynamic fatigue of soda-lime-silica float glass", *J. Am. Ceram. Soc.*, **85**, pp. 1777-1782, 2002.
8. J. Kim, S. Lee, J. Ahn and J. Lee, "AlN piezoelectric materials for wireless communication thin film components", *J. Ceramic Processing Research*, **3**, pp. 25-28, 2002.
9. K.M. Lakin, J. Belsick, J.F. McDonald and K.T. McCarron, "Improved bulk wave resonator coupling coefficient for wide bandwidth filters", *Proc. IEEE Ultrasonics Symposium 2001*, **1**, pp.827-831, 2001.
10. A. Choujaa, N. Tirole, C. Bonjour, G. Martin, D. Hauden, P. Blint, A. Cachard and C. Pommier, "AlN/silicon lamb-wave microsensors for pressure and gravimetric measurements", *Sensors and Actuators A* **46-47**, pp. 179-182, 1995.
11. T. Laurent, F.O. Bastien, J-C. Pommier, A. Cachard, D. Remiens and E. Cattan, "Lamb wave and plate mode in ZnO/ silicon and AlN/silicon membrane. Application to sensors able to operate in contact with liquid", *Sensors and Actuators A* **87**, pp. 26-37, 2000.
12. D. Ruffieux, M.A. Dubois and N.F. de Rooij, "An AlN piezoelectric microactuator array", *Proc. The Thirteenth Annual International Conference on Micro Electro Mechanical Systems 2000, IEEE MEMS 2000* , pp. 662-667, 2000.
13. K. Kusaka, D. Taniguchi, T. Hanabusa and K. Tominaga, "Effect of input power on crystal orientation and residual stress in AlN film deposited by DC sputtering", *Vacuum*, **59**, pp. 806-813, 2000.
14. C. Gorecki, M. Jozwik and L. Salbut, "Multifunctional interferometric platform for on-chip testing the micromechanical properties of MEMS/MOEMS", *J. Microlith., Microfab., Microsyst.*, **4**, 2005.
15. D. Malacara, M. Servin and Z. Malacara, *Interferogram analysis for optical testing*, Marcel Dekker Inc., New York, 1998.
16. E. Dianov, A. Kurkov, O. Medvedkov and S. Vasiliev, "A new sensitive method for measuring induced refractive index change in optical fiber core", *Proc. Int. Conf. Photosensitivity and Quadratic Non-Linearity in Glass Waveguides: Fundamentals and Applications, OSA Tech. Dig.*, **22**, Portland, Oregon, USA, 1995.
17. A. Fernandez Fernandez, B. Brichard and F. Berghmans , "In Situ Measurement of Refractive Index Changes Induced by Gamma Radiation in Germanosilicate Fibers", *IEEE Photonics Technology Letters*, **15**, pp. 1428-1430, 2003.
18. W. Gorski and M. Kujawinska, "Three-dimensional reconstruction of refractive index inhomogeneities in optical phase elements", *Optics and Lasers in Eng.*, **38**, pp. 373-385, 2002.
19. J. Hsieh, *Computed Tomography Principles, Design, Artifacts and Recent Advances*, SPIE Press monograph, **PM114**, 2003.
20. P. Kniazewski, W. Gorski and M. Kujawinska, "Microinterferometric tomography of photonics phase elements", *Proc. SPIE*, **5145**, pp. 107-116, 2003.
21. M. Kujawinska, "Spatial phase measurement methods", *Interferogram Analysis : Digital Fringe Pattern Measurement Techniques*, D.W. Robinson and G. Reid (eds.), pp. 141-193, Institute of Physics Publishing, 1993.
22. A. Fernandez Fernandez, H. Ooms, B. Brichard, M. Coeck, S. Coenen, F. Berghmans, and M. Décréton, "SCK-CEN irradiation facilities for radiation tolerance assessment," *Proc. IEEE NSREC 2002, Radiation Effects Data Workshop, July 2002, Phoenix, Arizona, USA*, pp. 171-176, 2002.

ACKNOWLEDGEMENTS

The work was performed within the EU FP6 Network of Excellence on Micro-Optics – NEMO. The Grant for Bilateral Scientific Cooperation between Poland and Flanders is acknowledged as well. The authors are also grateful for financial support of the Polish Ministry of Science and Information Technologies under Grant n°. 4T10C00425.